Identification of Defective CMOS Devices using Correlation and Regression Analysis of Frequency Domain Transient Signal Data

James F. Plusquellic*, Donald M. Chiarulli* and Steven P. Levitan†

*Department of Computer Science, University of Pittsburgh
†Department of Electrical Engineering, University of Pittsburgh

Abstract

Transient Signal Analysis is a digital device testing method that is based on the analysis of voltage transients at multiple test points and on I_{DD} switching transients on the supply rails. We show that it is possible to identify defective devices by analyzing the transient signals produced at test points on paths not sensitized from the defect site. The small signal variations produced at these test points are analyzed in the frequency domain. Correlation analysis shows a high degree of correlation in these signals across the outputs of defect-free devices. We use regression analysis to show the absence of correlation across the outputs of bridging and open drain defective devices.

1.0 Introduction

Transient Signal Analysis (TSA) is a parametric approach to testing digital integrated circuits. TSA is based on a measurement of the contribution to the transient response of a device by physical characteristics such as substrate, power supply or parasitic coupling which are present in any circuit. Defect detection is accomplished in TSA by analyzing the variations produced by defects in the voltage and current transients of defective devices. The voltage transients are measured on test points near the primary outputs of the device. The current transients can be measured at the power supply I/O pins of a device without significant high frequency attenuation because of the absence of driver circuitry in the pads. However, these signals alone cannot be used to differentiate between the variations produced by defects and those produced by variability in device characteristics due to process variations. TSA is able to distinguish between these two types of variations by additionally measuring voltage transients at a set of test points. The variations in multiple test point signals are cross-correlated to determine if the variation is regional or global. The absence of correlation in one or more of the test point signals indicates the presence of a catastrophic defect. On the other hand, the variations produced by fluctuations in process parameters tend to be global and correlated in all test point measurements.

In previous papers [1][2], we have demonstrated through simulations that global variations of major device performance parameters, i.e. threshold voltage and gate oxide thickness, result in measurable changes of the circuit's transient response at all test points. In contrast, the presence of a device defect will change both the value and topology of the parasitic components in the region of the defect. We have shown through other simulations that the changes introduced by both bridging and open drain defects result in measurable variations in the transient response and that these variations are distinct at two or more test points.

In this paper, we present the results from two hardware experiments conducted on devices with intentionally inserted bridging and open drain defects. We used test sequences that created logic faults in the defective devices, and measured the transient signals at test points both on and off the sensitized path from the defect site. We analyzed the frequency domain representations of the test point signals whose logic behavior was unchanged by the defect. The results of correlation analysis show that a high degree of correlation exists in the signals between test point pairings of defect-free devices. We use linear regression analysis to show that the regional signal variations produced by defects are not correlated with the signals of defect-free devices. The absence of correlation in one or more test point signals is used to identify the defective devices.

The remainder of this paper is organized as follows. In Section 2 we present related research and a discussion of the Transient Signal Analysis (TSA) method and model. Section 3 presents the results of hardware experiments conducted on devices with intentionally inserted bridging and open drain defects. Section 4 gives a summary and conclusions.

2.0 Background

Parametric device testing strategies [3][4] are based on the analysis of a circuit's parametric properties, for example, propagation delay, magnitude of quiescent supply current or transient response. Parametric methods have been shown to be more effective than conventional logic based methods in detecting common types of CMOS defects [5][6]. Many types of parametric tests have been proposed [7] but recent research interest has focused primarily on three types; I_{DDQ} [8], I_{DD} [9], and delay fault testing [10][11].

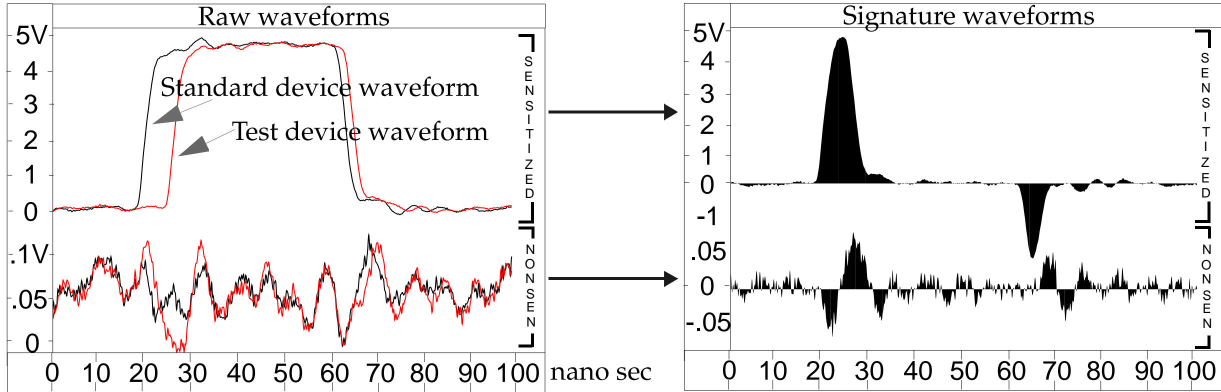

Figure 1. Time Domain Signature Waveform creation procedure.

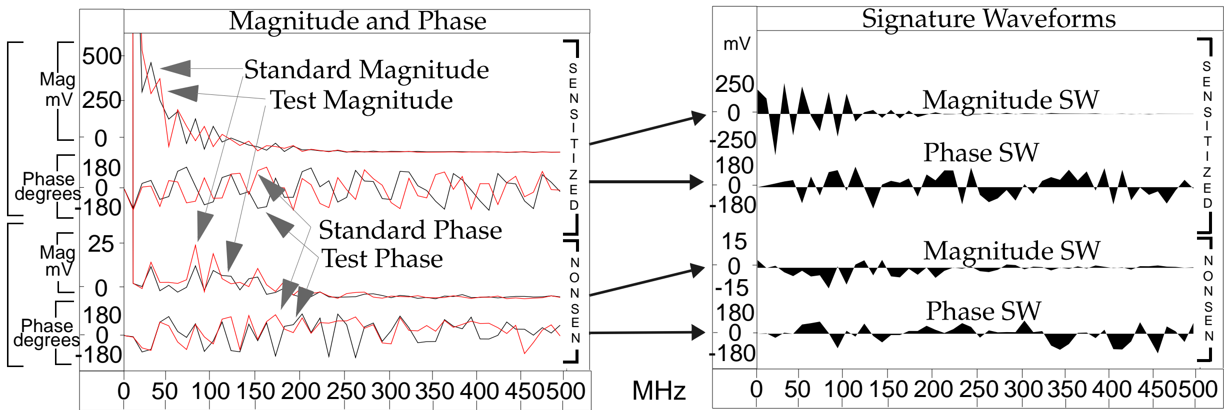

Figure 2. Frequency Domain Signature Waveform creation procedure.

I_{DDQ} is based on the measurement of an IC's supply current when all nodes have stabilized to a quiescent value [12]. I_{DDQ} has been shown to be an effective diagnostic technique for CMOS bridging defects, but is not applicable to all types of CMOS defects [13]. More recently, concerns have been raised over the applicability of I_{DDQ} to deep submicron technologies [14]. Several dynamic supply current (I_{DD}-based) approaches have since been proposed to overcome the limitations of the I_{DDQ} test [9][15][16][17][18]. However, these methods do not provide a means of accounting for changes due to process parameter variations and are therefore subject to aliasing problems.

Alternatively, delay fault testing is capable of detecting many common CMOS defects but test vector generation is complicated due to static and dynamic hazards [6][19][20]. Also, the effectiveness of a delay fault test is dependent on the propagation delay of the tested paths and the delay defect size [21]. Franco and McCluskey [22] and others [23][24][25] have proposed extensions to delay fault testing that address some of these difficulties.

Recently, Ma, *et al.* [26] and others [5][6][27][28] evaluated a large number of test methodologies and determined that a combination of several test strategies may be necessary in order to find all defective devices. In particular, Ma, *et al.* discovered that I_{DDQ} cannot detect all kinds of defects and must be used with some kind of dynamic voltage test. Our technique, Transient Signal Analysis (TSA), with its advantages in defect detection and process insensitivity, is proposed as an addition to this test suite.

TSA is based on the analysis of transient signal variations. In order to capture the variations produced by defects and process parameter fluctuations in the test point signals, we create Signature Waveforms using the procedure shown in Figure 1. Shown in the upper portion of the left plot of Figure 1 are the transient waveforms generated by two devices at a test point located along a sensitized test path. Similarly, shown along the bottom are two transient waveforms produced by the same two devices at a non-sensitized test point. **Signature Waveforms** (**SWs**) are created from these pairs of transient waveforms by subtracting the Test device waveform from the Standard device waveform. The difference waveforms, shown in the right plot of Figure 1, are then shaded along a zero baseline to add emphasis to the variations. The frequency domain SWs are created by performing a discrete fourier transform (DFT) on the raw time domain waveforms as shown in Figure 2. Magnitude and phase SWs are created from the DFT's out-

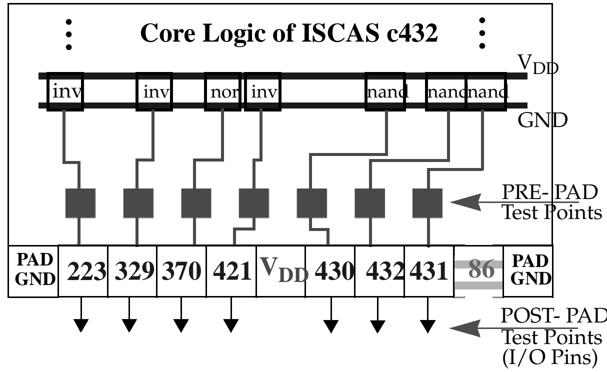

Figure 3. Location of the test points on the c432.

put by subtracting the test device magnitude and phase values from the corresponding values of the standard device.

3.0 Experiments

In this section we present the results of two hardware experiments that demonstrate that it is possible to identify defective devices by analyzing the frequency domain Signature Waveforms. The experiments were conducted on three different versions of the ISCAS85 c432 benchmark circuit [29], a version with intentionally inserted bridging defects, a version with intentionally inserted open drain defects and a defect-free version. Four devices of each version were fabricated at MOSIS using ORBIT's 2.0μm SCNA process. The defect-free devices were verified using both functional and Stuck-At test sets.

A digitizing oscilloscope with a bandwidth of 1 GHz was used to collect a 2048 point waveform from each of the test points. The averaging function of the oscilloscope was used to reduce ambient noise levels. The experiments were run at 11 MHz, about half the maximum clock rate of the devices.

The test points used in these experiments are labeled PRE-PAD and POST-PAD in Figure 3. The POST-PAD experimental results are described in [30]. The PRE-PAD test points are 22 micron square Metal 2 pads placed on the output nodes of the gates driving the seven primarily outputs of the c432. Since these test points are not driven by the I/O pad drivers, variation caused by coupling through the power supply lines of the pads has been minimized. In addition, the high frequency components of the signals generated through the core logic coupling mechanisms has been preserved. The measurements were taken at a probe station using a PicoProbe, model 12C, with a 100 FF and 1 MΩ load.

In each experiment four non-defective and four defective devices were tested. The TSA testing process involves applying a test vector sequence to the primary inputs (PIs) of an IC and sampling the waveforms generated at the test points. In order to extract only the variation that occurs between the test devices and the standard device, Signature Waveforms were created in both the time and frequency domain. The same defect-free standard device was used to create all SWs shown in this paper.

3.1 Bridging Experiment

The results of the bridging experiment are shown in this section. Figure 4 shows a portion of the schematic diagram of the c432. Only those sensitized paths affected by the defect are shown. The input stimulus for this experiment toggles PI 66 at 11MHz. PI 56 is held high and the other PIs (not shown) are held low. The dotted line in the figure represents the bridging defect which was created in the layout by inserting a first-level to second-level metal contact between the output lines of the 4-input NAND and the inverter. This simulates an SiO_2 defect. The only PO that changes logic state is 370. However, in the defect-free circuit, a static hazard causes a pulse to propagate to POs 421 and 430 along the shaded paths in the figure. Note that the bridging defect is not on any sensitized path and no contention exists between the two bridged nodes in steady-state. However, since the output of the inverter driven by PI 56 is low, the bridge eliminates the pulse produced by the hazard in the defective circuit.

Only a selected set of Signature Waveforms are shown and the reader is directed reference [31] for an extended presentation of these results. Each of the plots in Figure 5 shows a set of time domain or frequency domain SWs from a single test point. The time domain SWs are always shown in the left-most plot while the magnitude and phase are shown in the middle and right-most plots respectively. Each row across the three plots represents the time and frequency domain SWs produced by a single device at the test point identified in the figure header. The top-most waveform of each plot is the output trace from the standard IC used in the difference operation to create the SWs shown below it. The next three waveforms labeled DF#*x* are the SWs from each of the three *Defect-Free* ICs. The next four SWs, labeled either BR#*x* for *BRidging* defects or OD#*x* for *Open Drain* defects are the SWs from the four defective ICs.

The SWs generated on POs 421 and 430 are not considered in the analysis that follows. Defective device identification using the SWs of these outputs is trivial due to the presence of large signal variation. The objective of this experiment and the next is to determine if the small signal variations on test points not sensitized from the defect site can be used to distinguish between the defect-free and defective devices. For this experiment, we will analyze the SWs produced on POs 223, 329, 370, 431, 432 and I_{DD}.

As indicated in the schematic diagram of Figure 4, POs 223 and 329 are held high and POs 431 and 432 are held low under this test sequence. The SWs produced on

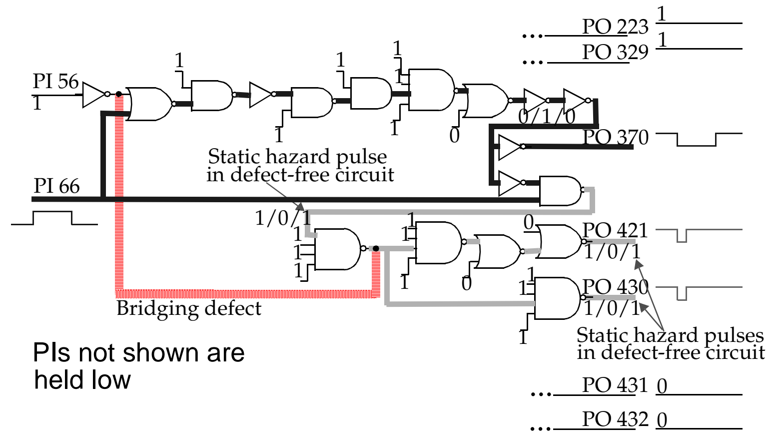

Figure 4. Portions of the c432 schematic showing the short and the sensitized paths affected by the defect in the Bridging Experiment.

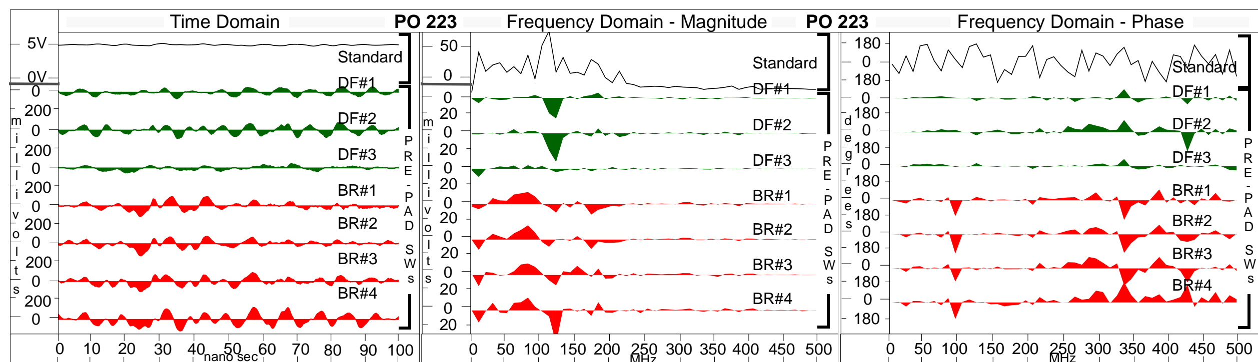

Figure 5. Time and Frequency domain Signature Waveforms from PO 223 of Bridging Experiment.

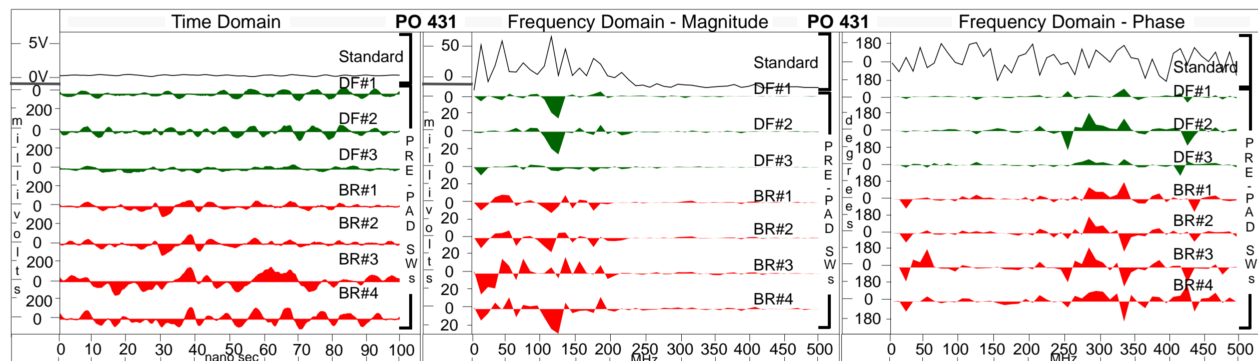

Figure 6. Time and Frequency Domain Signature Waveforms from PO 431 of Bridging Experiment.

POs 223 and 431 are shown in Figures 5 and 6. The SWs generated on POs 329 and 432 are very similar to those shown in Figures 5 and 6 respectively and are not shown. The characteristic that we seek in the SWs of any one plot is a distinguishing feature in the SWs of the defective devices that does not appear in the SWs of the defect-free devices. Given this objective, three observations can be made concerning the SWs shown in the figures.

First, it is not clear that the BR#x SWs are different than the DF#x SWs in the time domain plots shown on the left in the figures. Second, the magnitude SWs of the defective devices shown in the middle plots of these figures show distinguishable variation in the region between 50 and 100 MHz. But the variation in the magnitude SWs of DF#1 and DF#2 around 125 MHz create an anomaly in the characterization of the defect-free devices. However, this anomaly can be attributed to fluctuations of process parameters if the magnitude SWs of POs 223 and 329 as well as POs 431 and 432 are considered together. This is true because the variation is global in that it occurs at the same frequency and with the same relative magnitude in all four test point SWs. Third, the phase shifts that occur in the defective device SWs shown on the right in the figures meet the objective described above in that they show dis-

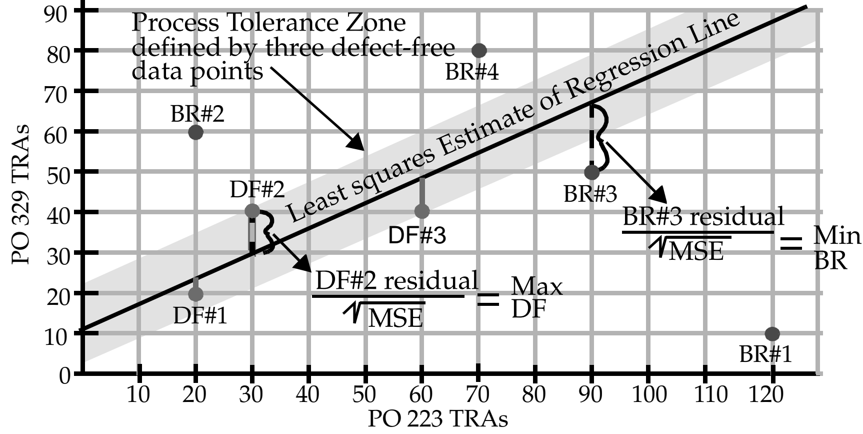

Figure 7. Example Scatter Plot showing "Max DF" and "Min BR" statistics reported in the tables.

Given a sample $[(X_1, Y_1), (X_2, Y_2),...,(X_n, Y_n)]$ is a random sample of n paired values of the random variables X and Y. The sample correlation coefficient is:

$$CC = \frac{\sum (X_i - \bar{X})(Y_i - \bar{Y})}{\left[\sum (X_i - \bar{X})^2 \sum (Y_i - \bar{Y})^2\right]^{1/2}} \qquad -1 \le CC \le 1.$$

A test statistic for testing the NULL hypothesis of zero correlation between X and Y

$$t^* = \frac{CC\sqrt{n-2}}{\sqrt{1 - CC^2}} \qquad \text{p-value} = 2P\{t(n-2) > t^*\}$$

Given a sample $\{(X_1, Y_1), (X_2, Y_2),...,(X_n, Y_n)\}$ of paired values from random variables X and Y, least squares estimate of the regression line is: $\hat{Y} = b_0 + b_1 X$ where:

$$b_1 = \frac{\sum (X_i - \bar{X})(Y_i - \bar{Y})}{\sum (X_i - \bar{X})^2} \qquad b_0 = \bar{Y} - b_1 \bar{X}$$

Sample variance in regression, MSE, is defined as:

$$MSE = \frac{\sum_{i=1}^{n} (Y_i - \hat{Y})^2}{n-2}$$

Figure 8. Expressions for the correlation coefficient, p-value, regression line and sample variance.

tinguishable features. For example, phase shifts occur in the phase SWs of devices BR#1 through BR#4 at 100 MHz on PO 223 and between 15 and 20 MHz on PO 431. No significant variation occurs in the phase SWs of the defect-free devices below 250 MHz. We believe that this change in phase variation between POs 223 and 431 is attributable to the difference in the capacitance loading to substrate of the V_{DD} and GND supply networks. In summary, these results indicate that the defect both delays and distorts specific frequency components of off-path signals. This phenomena is difficult to see in the time domain SWs shown in the left-most plots of Figures 5 and 6 because other frequency components of the transient signals combine to mask these variations.

The SWs generated on POs 370 and I_{DD} are not shown but are used in the correlation analysis that follows. The variations in the SWs of PO 370 are dominated by the variations caused by process parameter fluctuation and consequently, the regional variation produced by the defect are more difficult to observe. This result and the results shown for the non-sensitized POs 223 and 431 suggest that the regional variation caused by a defect is most easily measured on steady-state test points. We will confirm this observation in the analysis that follows.

3.2 Correlation and Linear Regression Analysis

In this section, we describe a statistical method that we use to identify the defective devices. The analysis is based on the area computed under the shaded portion of the SWs shown in Figures 5 and 6. The shaded area up to 250MHz is computed for each magnitude and phase Signature Waveform using a Trapezoidal Rule integration method. We will use Trapezoidal Rule Area (TRA) to refer to the computed area value. While this procedure discards information regarding the frequency at which the variations occur, we show that this method is still able to capture the important information in the SWs and allow the defective devices to be identified.

Figure 7 depicts a Scatter Plot for an example test point pair 223 and 329 where the x and y axis are in units of TRA. The defect-free device data points are labeled DF#x while the bridging defective device data points are labeled BR#x. For example, the TRA computed on test point 223 for DF#3 is 60 and the corresponding TRA computed for that same device on test point 329 is 40. If it is true that the TRAs produced by global variations in process parameters are proportional across outputs then we would expect the DF#x data points to be nearly colinear. Therefore, the defect-free device TRA data points define a region that

Output Pair	MAG CC	p-value	Max DF	Min BR	BR Device	# other BRs	PHASE CC	p-value	Max DF	Min BR	BR Device	# other BRs
223/329	+1.000	0.013	**-0.793**	**27.622**	BR#1	0	+0.997	0.047	**0.718**	**-9.004**	BR#4	0
223/370	+0.820	0.388	-0.793	0.107	BR#3	0	+1.000	0.002	**-0.718**	**-375.114**	BR#3	0
223/431	+0.999	0.032	**0.793**	**3.917**	BR#4	0	+0.979	0.130	**0.718**	**-4.016**	BR#2	0
223/432	+0.995	0.062	**0.793**	**2.611**	BR#4	0	+0.996	0.056	**0.718**	**11.800**	BR#3	0
223/IDD	+0.975	0.142	**0.793**	**7.279**	BR#2	0	+0.990	0.091	**-0.718**	**1.146**	BR#2	0
329/370	+0.832	0.375	**-0.796**	**0.839**	BR#4	0	+0.997	0.048	**-0.745**	**-19.506**	BR#1	0
329/431	+0.998	0.044	**0.796**	**-6.853**	BR#4	0	+0.992	0.083	**0.745**	**-4.739**	BR#1	0
329/432	+0.993	0.075	0.796	0.078	BR#2	0	+1.000	0.009	**0.745**	**-51.104**	BR#1	0
329/IDD	+0.971	0.155	**0.796**	**1.188**	BR#2	0	+0.977	0.138	**-0.745**	**-4.714**	BR#2	0
370/431	+0.791	0.419	0.762	-0.010	BR#4	1	+0.979	0.131	**0.717**	**4.252**	BR#1	0
370/432	+0.761	0.450	0.762	0.188	BR#4	0	+0.996	0.057	**0.717**	**8.771**	BR#1	0
370/IDD	+0.673	0.530	**0.762**	**3.511**	BR#2	0	+0.990	0.090	**-0.717**	**17.160**	BR#2	0
431/432	+0.999	0.030	**0.782**	**1.148**	BR#4	0	+0.993	0.074	-0.782	0.264	BR#4	1
431/IDD	+0.985	0.110	**0.782**	**10.804**	BR#2	0	+0.940	0.221	**-0.782**	**-2.687**	BR#3	0
432/IDD	+0.992	0.080	**0.770**	**1.923**	BR#2	0	+0.973	0.147	**-0.749**	**3.697**	BR#3	0

Table 1: Correlation and linear regression analysis of magnitude and phase areas for Bridging experiment.

tracks process variation, labeled “Process Tolerance Zone” in the figure. In contrast, the BR#x TRAs additionally capture the regional variation produced by defects and generate data points that fall outside of this region. This is true because the signal variations produced by defects are different, depending on the logic state and location of the test point with respect to the defect site.

We demonstrate that it is possible to identify defective devices by showing that most pairings of their test point TRAs produce data points that fall well outside of the band that tracks process variation. We first compute a correlation coefficient using the TRAs of the defect-free (DF#x) SWs for each pairing of the outputs. This value and its p-value will determine the degree of linear association that exists in the TRAs across the devices. Correlation coefficients close to -1.00 or +1.00 and corresponding p-values less than 0.05 indicate that the TRAs across the outputs of defect-free devices are significantly correlated. We also compute an estimate of the regression line through the DF#x data points, using the Least Squares method. The residuals of the DF#x and BR#x data points are computed and standardized using the standard deviation of the DF#x residuals. The maximum ZRES (Standardized Residual) produced by one of the DF#x devices and the minimum ZRES produced by one of the BR#x devices are reported in the tables. An example of this procedure is shown in Figure 7. In this example, the ZRES values of data points DF#2 and BR#3 would be reported in the table under the column headings “Max DF” and “Min BR”, respectively. Expressions for computing the correlation coefficient (CC), the p-value, the regression line and the sample variance are shown in Figure 8. Sample variance, MSE, was computed using the residuals of the DF#x devices only.

Table 1 shows the results from the bridging experiment. The first column identifies the output pair whose data is given on the row. The remaining 12 columns are split in half with a double vertical line. The 6 columns to the left of the dividing line show the magnitude results while the 6 columns on the right show the phase results. The correlation coefficient (MAG CC and PHASE CC) and its p-value are shown in the first two of each 6 column pair. The Max DF and Min BR columns show the ZRES values as described above. The last 2 columns show the BR device whose ZRES value is closer than the maximum among the defect-free devices and the number of other defective devices for which this condition is true.

The shaded blocks in the table show the number of instances in which the maximum ZRES value of the defect-free devices is less than the minimum ZRES value of the defective devices. In other words, for these rows, the data points of all four defective devices are located outside the shaded zone shown in Figure 7 which tracks process varia-

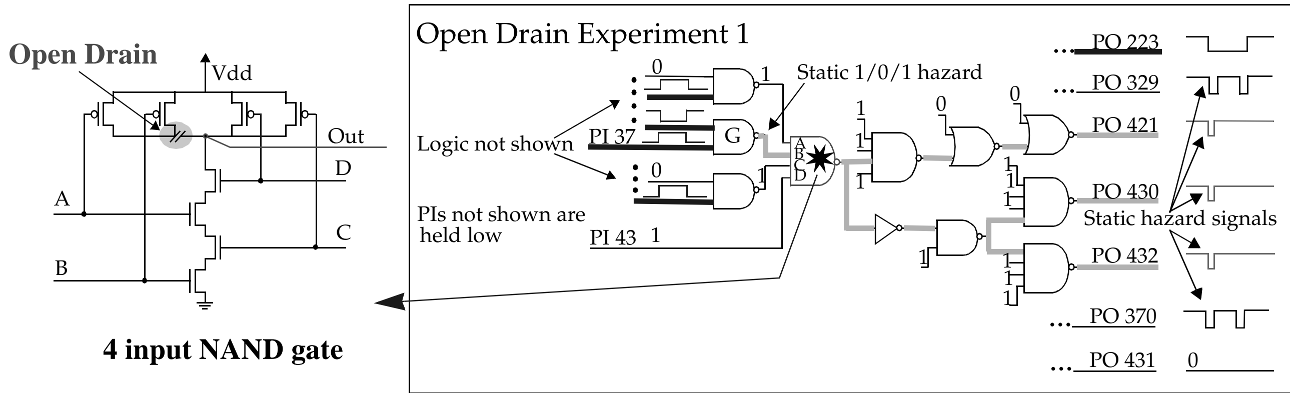

Figure 9. Portions of the c432 schematic showing the sensitized paths for the Open Drain experiment.

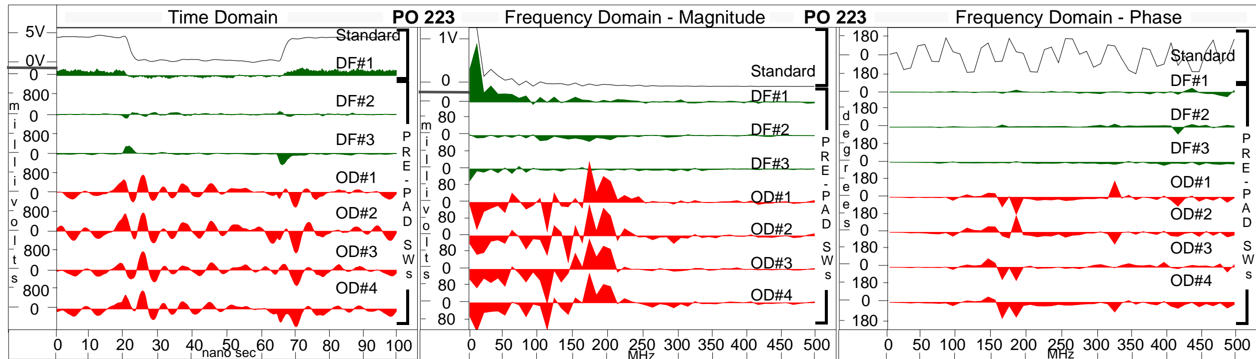

Figure 10. Time and Frequency Domain Signature Waveforms from PO 223 of Open Drain Experiment.

tion. The phase results are more useful than the magnitude results in all aspects of the statistics. First we note that of the fifteen rows, eleven of them are shaded for magnitude while fourteen are shaded for phase. Also, the smallest phase correlation coefficient is 0.940 while five of the magnitude correlation coefficients are less than 0.900. In either case, however, the defective devices can be identified. Also, for the magnitude analysis, no defective device had more than two of the fifteen data points that fell within the shaded zone and all devices had at least three data points that were twenty times larger than the "Max DF" ZRES value. For the phase analysis, no defective device had more than one of the fifteen data points that fell within the shaded zone and all devices had at least two data points that were fifty times larger than the "Max DF" ZRES value.

3.3 Open Drain Experiment

The results of an open drain experiment are presented in this section. Figure 9 shows the sensitized paths through the defective gates for the open drain experiments. The left side of Figure 9 shows an open drain defect in the transistor-level schematic diagram of a 4-input NAND gate. A three micron wide piece of first-level metal has been removed between the p-transistor drain pairs. The test sequence for the first experiment generates a number of pulses at the POs which are created by a static hazard. The difference in the signal arrival times on the inputs to the NAND gate labeled G in Figure 7 cause the output of the gate to pulse low in the non-defective circuit. Since gate G drives input B of the 4-input NAND gate, the static hazard signals are not generated in the defective circuit.

The SWs generated on POs 421, 430 and 432 are not considered in the analysis that follows. As was true in the Bridging experiment, the identification of the defective devices would be trivial using the SWs of these outputs due to the presence of large signal variation. Again, the emphasis of this experiment is on the small signal variations produced at test points not sensitized from the defect site. Consequently, we will analyze the SWs produced on POs 223, 329, 370, 431 and I_{DD}.

As indicated in Figure 7, the path driving PO 223 is sensitized and the paths driving POs 329 and 370 propagate hazard signals in both the defective and defect-free devices. Figure 10 shows the SWs generated on PO 223. Observations similar to those made in the Bridging experiment can be made here except that the time domain SWs provide a better visual clue as to which devices are defective. However, the SW of defect-free device DF#1 is significantly different than the other time domain SWs, defect-free or defective. Part of the 11MHz fundamental is present in this measurement. In fact, most of the variation in this SW is due to a measurement error which occurred because the probe tip was not firmly placed on the Metal 2 pad. This

Output Pair	MAG CC	p-value	Max DF	Min OD	OD Device	# other ODs	PHASE CC	p-value	Max DF	Min OD	OD Device	# other ODs
223/329	-0.423	0.722	**0.743**	**3.170**	OD#3	0	-0.355	0.769	**0.772**	**3.377**	OD#3	0
223/370	-0.272	0.825	**0.743**	**0.926**	OD#4	0	-0.429	0.718	**0.772**	**3.366**	OD#3	0
223/431	-0.799	0.410	**0.743**	**12.008**	OD#1	0	-0.415	0.727	**0.772**	**18.501**	OD#1	0
223/IDD	-0.779	0.432	**0.743**	**5.524**	OD#2	0	-0.384	0.749	**0.772**	**4.034**	OD#3	0
329/370	+0.987	0.103	**-0.710**	**-7.112**	OD#3	0	+0.997	0.051	**0.719**	**-7.420**	OD#3	0
329/431	+0.883	0.311	**0.710**	**4.383**	OD#1	0	+0.998	0.042	**0.719**	**192.790**	OD#1	0
329/IDD	+0.898	0.290	**0.710**	**-3.038**	OD#2	0	+1.000	0.020	**0.719**	**-3.607**	OD#1	0
370/431	+0.796	0.414	**-0.761**	**8.879**	OD#1	0	+1.000	0.009	**-0.747**	**905.200**	OD#1	0
370/IDD	+0.815	0.393	**-0.761**	**2.545**	OD#2	0	+0.999	0.031	**-0.747**	**10.284**	OD#1	0
431/IDD	+0.999	0.021	**-0.816**	**-11.726**	OD#3	0	+0.999	0.022	**-0.743**	**-328.720**	OD#2	0

Table 2: Correlation and linear regression analysis of magnitude and phase areas for Open Drain experiment.

type of measurement error may be common so it is important to know whether or not we can identify such errors using our statistical procedure.

The SWs for POs 329, 370, 431 and I_{DD} are not shown but they too show distinguishable characteristics between the defect-free and defective devices. It is also interesting to note the distinctive phase shifts that occur in the phase SWs shown in Figure 10 for the defective devices, in this case over the frequency range between 150 and 200 MHz.

The results of the correlation and linear regression analysis for this experiment are shown in Table 2. The correlation coefficients for the magnitude analysis are lower than those for the bridging experiment. They are very low for output pairs 223/329 and 223/370 because of the additional variation produced by the measurement error. The overall reduction in correlation coefficients is due to the mixture of transitioning and non-transitioning test point signals in this experiment. In general, the correlation of test point signals within sets of transitioning or sets of non-transitioning test point signals is higher than the correlation of test point signals between these sets. It is also true that higher degrees of correlation are observed when I_{DD} is paired with non-transitioning test points. For example, the correlation coefficient for output pair 431/I_{DD} is +0.999. PO 431 is a steady-state low signal under the test sequence used in this experiment. In contrast, the correlation coefficients for output pairs 329/I_{DD} and 370/I_{DD} are +0.898 and +0.815, respectively. However, there is high correlation in output pair 329/370. As noted in the Figure 9, both of these test points transition. Similar observation can also be made for the Bridging experiment results shown in Table 1.

Given this trend, we would expect the 223 output pairs to have higher correlation coefficients for pairing with POs 329 and 370 than with PO 431 and I_{DD}. However, the expected trend is in fact reversed in the results which suggests that a measurement error may have occurred. Independent of the error, all rows are shaded indicating that none of the defective device data points fell into the shaded zone defined by the defect-free devices. This shows the robustness of the method even when significant amounts of measurement error are present.

Similar to the bridging experiment, the results of the phase analysis for this experiment are more useful than the results shown for the magnitude analysis. The correlation coefficients shown on the left side of Table 2 provide a clear indication that a problem exists in the SWs generated on PO 223. The correlation coefficients shown for the output pairs that do not include PO 223 are all greater than +0.997. The reduction of correlation between transitioning and non-transitioning test points that we noted in the magnitude correlation coefficients of both experiments does not occur in the phase results. Similar to the magnitude results, all rows are shaded in this experiment which allows the defective devices to be identified.

4.0 Summary and Conclusions

The hardware experiments conducted on the c432 have shown that the variations produced by defects and fluctuations in fabrication process parameters are measurable in the transient signals of devices. These variations are extracted by computing a difference waveform called a Signature Waveform. We have shown that defects cause measurable variations to occur in Signature Waveforms generated on test points not sensitized from the defect site. By measuring the variations that occur at multiple test

points simultaneously, we have also demonstrated that we can distinguish between the variations produced by defects and those that are produced by natural changes in fabrication process parameters. The results of a correlation analysis have shown that the latter variation is proportional in area across the test point Signature Waveforms of defect-free devices. The results of linear regression analysis have shown that it is possible to identify defective devices by observing the absence of correlation in the areas computed across one or more Signature Waveforms of the defective devices.

These results also indicate that the variations caused by defects are most easily measured as phase shifts in the frequency domain. The correlation and regression line analysis support this result in that the phase correlation coefficients for the defect-free devices are consistently closer to the ideal value of 1.00 than those shown for the magnitude. This means that the widths of the process variation bands are narrower in the phase analysis. Also, the standardized residual values for the defective devices are larger in the phase analysis than in the magnitude analysis. Consequently, the phase analysis provides a more sensitive defect detection test.

In addition, these experimental results show that the correlation coefficients computed in the magnitude analysis are smaller for output pairs containing one test point that transitions and one that does not. This suggests that the accuracy of the magnitude analysis may be improved by restricting the correlation analysis to output pairs that either both transition or remain in steady-state.

The open drain experiment further demonstrates the robustness of the method to measurement error and that it may be possible to identify measurement error due to the anomalies that are created in the correlation coefficients.

We are currently investigating a means of quantifying the degree of coupling through each of the main parasitic coupling mechanisms, namely, power supply, internodal, well and substrate when defects are introduced into neighboring circuit components. This information and other simulation experiments will help us determine the number and position of the test points or the amount of observability required and subsequently, the number and type of test vectors necessary to achieve a given fault coverage.

References

[1] James F. Plusquellic, Donald M. Chiarulli, and Steven P. Levitan. Digital IC device testing by transient signal analysis (TSA). *Electronics Letters*, 31(18):1568–1570, August 1995.

[2] James F. Plusquellic, Donald M. Chiarulli, and Steven P. Levitan. Simulation of Digital IC Transient Response in Defective and Defect-Free devices. *Technical Report TR 96-12,* Department of Computer Science, University of Pittsburgh, July, 1996.

[3] Mark W. Levi. CMOS is Most Testable. In *IEEE Test Conference*, pages 217-220, 1981.

[4] F. Joel Ferguson, Martin Taylor and Tracy Larrabee. Testing for Parametric Faults in Static CMOS Circuits. In *International Test Conference*, pages 436-443, 1990.

[5] Charles F. Hawkins, Jerry M. Soden, Alan W. Righter and Joel Ferguson. Defect Classes - An Overdue Paradigm for CMOS IC Testing. In *International Test Conference*, pages 413-425, 1994.

[6] Jerry M. Soden and Charles F. Hawkins. Electrical properties and detection methods for CMOS IC defects. In *Proceeding of the European Test Conference*, pages 159–167, 1989.

[7] A. P. Dorey, B. K. Jones, A. M. D. Richardson, and Y. Z. Xu. *Rapid Reliability Assessment of VLSICs*. Plenum Press, 1990.

[8] Thomas M. Storey and Wojciech Maly. CMOS bridging fault detection. In *International Test Conference*, pages 1123–1132, 1991.

[9] James F. Frenzel and Peter N. Marinos. Power supply current signature (PSCS) analysis: A new approach to system testing. In *International Test Conference*, pages 125–135, 1987.

[10] E. P. Hsieh, R. A. Rasmussen, L. J. Vidunas, and W. T. Davis. Delay test generation. In *Proceeding of the 14th Design Automation Conference*, pages 486–491, 1977.

[11] Chin Jen Lin and S. M. Reddy. On delay fault testing in logic circuits. *IEEE Transactions on Computer-Aided Design*, CAD-6(5):694–703, September 1987.

[12] Steven D. McEuen. I_{DDQ} benefits. In *VLSI Test Symposium*, pages 285–290, 1991.

[13] Adit D. Singh, Haroon Rasheed, and Walter W. Weber. I_{DDQ} testing of CMOS opens: An experimental study. In *International Test Conference*, pages 479–489, 1995.

[14] E. McCluskey(Moderator), K. Baker(Organizer), W. Maly, W. Needham, M. Sachdev(Panelists), “Will I_{DDQ} Testing Leak Away in Deep Sub-Micron Technology?”, *International Test Conference*, Panel 7, 1996.

[15] M. Hashizume, K. Yamada, T. Tamesada, and M. Kawakami. Fault detection of combinatorial circuits based on supply current. In *International Test Conference*, pages 374–380, 1988.

[16] A. P. Dorey, B. K. Jones, A. M. Richardson, P. C. Russel, and Y. Z. Zu. Reliability testing by precise electrical measurement. In *International Test Conference*, pages 369–373, 1988.

[17] J. S. Beasley, H. Ramamurthy, J. Ramirez-Angulo, and M. DeYong. I_{DD} pulse response testing of analog and digital CMOS circuits. In *International Test Conference*, pages 626–634, 1993.

[18] Rafic Z. Makki, Shyang-Tai Su, and Troy Nagle. Transient power supply current testing of digital CMOS circuits. In *International Test Conference*, pages 892–901, 1995.

[19] Ankan K. Pramanick and Sudhakar M. Reddy. On the detection of delay faults. In *International Test Conference*, pages 845–856, 1988.

[20] Alicja Pierzynska and Slawomir Pilarski. Non-Robust versus Robust. In *International Test Conference*, pag-

es 123-131, 1995.

[21] E. S. Park, M. R. Mercer, and T. W. Williams. Statistical delay fault coverage and defect level for delay faults. In *International Test Conference*, pages 492–499, 1988.

[22] Fiero Franco and Edward J. McCluskey. Delay testing of digital circuits by output waveform analysis. In *International Test Conference*, pages 798–807, 1991.

[23] A. Chatterjee, R. Jayabharathi, P. Pant and J. A. Abraham. Non-Robust Tests for Stuck-Fault Detection Using Signal Waveform Analysis: Feasibility and Advantages. In *VLSI Test Symposium,* pages 354-359, 1996.

[24] A. Wu, T. Lin, C. Tseng, and J. Meador. Neural network diagnosis of IC faults. In *VLSI Test Symposium*, pages 199–203, 1991.

[25] C. Thibeault. Detection and location of faults and defects using digital signal processing. In *VLSI Test Symposium*, pages 262–267, 1995.

[26] Siyad C. Ma, Piero Franco, and Edward J. McCluskey. An experimental chip to evaluate test techniques: Experiment results. In *International Test Conference*, pages 663–672, 1995.

[27] Peter C. Maxwell, Robert C. Aitken, Vic Johansen and Inshen Chiang. The effectiveness of I_{DDQ}, Functional and Scan Tests: How many fault coverages do we need? In *International Test Conference*, pages 168-177, 1992.

[28] Christopher L. Henderson, Jerry M. Soden and Charles F. Hawkins. The behavior and testing implications of CMOS IC logic gate open circuits. In *International Test Conference*, pages 302-310, 1991

[29] F. Brglez and H. Fujiwara. A neutral netlist of 10 combinational benchmark circuits and a target translator in FORTRAN. *Special Session on ATPG and Fault Simulation, Int. Symposium on Circuits and Systems*, pages 663-698, June 1985.

[30] James F. Plusquellic, Donald M. Chiarulli, and Steven P. Levitan. “Digital Integrated Circuit Testing using Transient Signal Analysis,” *International Test Conference*, pp. 481-490, October 1996.

[31] James F. Plusquellic, Donald M. Chiarulli, and Steven P. Levitan. Time and Frequency Domain Transient Signal Analysis for Defect Detection in CMOS Digital ICs. *Technical Report TR 97-07,* Department of Computer Science, University of Pittsburgh, May, 1997.